Microfluidics and Nanofluidics (2024) 28:3
https://doi.org/10.1007/s10404-023-02699-4

RESEARCH

Co-printing of micro/nanostructures integrated with preconcentration to enhance protein detection

Yi-Jung Lu[1] · Han-Yun Hsieh[2,3,4] · Wen-Fai Yang[2] · Kuang-Chong Wu[2] · Hidetoshi Tahara[3] · Pei-Kuen Wei[5] · Horn-Jiunn Sheen[2] · Yu-Jui Fan[4]

Received: 1 June 2023 / Accepted: 8 November 2023 / Published online: 9 December 2023

Abstract

This paper reports a fabrication method that can make microstructures such as microfluidic channels and nanostructures to generate surface plasmon resonance (SPR) signals in one-step using hot embossing. We first made a micro/nanostructural mold on a silicon substrate through sequential e-beam lithography, reactive ion etching (RIE), photolithography, and inductively coupled plasma RIE. The fabricated mold and cyclo-olefin polymer (COP) film were pressed between two flat, heated metal bases under optimal conditions, and the micro/nanostructures were complementarily transferred to the COP film. After depositing a thin aluminum film onto the nanostructure, the device was completed by patterning Nafion that crossed two channels and a nearby nanostructure, and by bonding the COP film to a flat polydimethylsiloxane (PDMS) substrate with holes punched for the inlets and outlets. SPR signals of the nanostructures of the microfluidic channel were calibrated using glycerol solutions of different percentages, and a wavelength sensitivity of 393 nm/refractive index unit was found for the Al-based nanoslit SPR sensing chip. To detect macromolecules, we first modified bovine serum albumin (BSA) onto the surface of the SPR chip and then allowed different concentrations of anti-BSA samples to flow into the device. A calibration curve for detecting anti-BSA was constructed, and anti-BSA detection levels with and without preconcentration were compared.

Keywords Localized surface plasmon resonance (LSPR) · Biosensor · Microfluidics · Hot embossing · Ion concentration polarization

1 Introduction

Surface plasmon resonance (SPR) effects are widely used in biomedical applications, that are mainly focused on biosensors (Homola et al. 1999; Homola and Piliarik 2006; Lee et al. 2016; Masson 2017; Yougbaré et al. 2020, 2021). Conventional SPR is based on the principle of detecting changes in the refractive index near the surface of a thin metal film. When light propagates through a prism onto a metal film with a total refraction angle, surface plasmon is generated at the metal surface. The angle at which this occurs is known as the resonance angle. The technique can be used to detect interactions between biomolecules in real time (Singh 2016; Zhou et al. 2019; Mahmoudpour et al. 2019; Das et al. 2023). When biomolecules bind to the surface of a metal film, they cause a change in the refractive index near the surface which results in a shift in the resonance angle.

Localized SPR (LSPR) can detect changes in the refractive index near the surface of a metal nanostructure (Sherry et al. 2005; Zhao et al. 2006; Mousavi et al. 2015; Lee et al.

Yi-Jung Lu and Han-Yun Hsieh are equally contributed.

✉ Pei-Kuen Wei
pkwei@sinica.edu.tw

✉ Horn-Jiunn Sheen
sheenh@ntu.edu.tw

✉ Yu-Jui Fan
ray.yj.fan@tmu.edu.tw

[1] Division of Family and Operative Dentistry, Department of Dentistry, Taipei Medical University Hospital, 252 Wuxing St., Taipei 11031, Taiwan

[2] Institute of Applied Mechanics, National Taiwan University, 1 Roosevelt Road, Sec. 4, Taipei 106, Taiwan

[3] Graduate School of Biomedical & Health Sciences, Hiroshima University, Kausmi 1-2-3, Minami-Ku, Hiroshima 734-8553, Japan

[4] School of Biomedical Engineering, Taipei Medical University, 250 Wuxing St., Taipei 11031, Taiwan

[5] Research Center for Applied Sciences, Academia Sinica, 128 Academia Road, Sec. 2, Nankang, Taipei 11529, Taiwan

2015, 2019; Yougbaré et al. 2020; Tan et al. 2021; Dutta et al. 2022; Mostufa et al. 2022). When light propagates into the nanostructure with sizes smaller than or comparable to the wavelength of the incident light, LSPR is generated in the near field of the nanostructure. Recently, a periodic submicron metallic grating film was designed to generate LSPR signals (Ebbesen et al. 1998; Lezec et al. 2002; Stewart et al. 2008). The resonant wavelength is known as the period of the grating time surrounding the refractive index. To mass-produce SPR sensing chips, grating structures are nano-imprinted onto plastic substrates, and then a thin metal film is deposited onto them (Lee et al. 2012; Hsieh et al. 2022a). This fabrication method allows mass-production and is also able to integrate the SPR chip with a microfluidic channel and miniaturization of the optical system (Hsieh et al. 2022b).

Integration of SPR into microfluidic channels has enabled the development of portable, low-cost SPR biosensors (Chuang et al. 2020; Wang et al. 2020). The combination of SPR biosensors and microfluidics has also enabled the development of high-throughput screening platforms for drug discovery.

Recently, nanofluidic preconcentration, based on integrated ion concentration polarization (ICP) phenomena, was developed with biosensors to detect low-abundance biomolecules (Wang et al. 2005; Ko et al. 2012; Chung et al. 2015; Deng et al. 2018; Fan et al. 2018; Sheen et al. 2022). ICP is an electrokinetic phenomenon that occurs in a selective ion channel that bridges two parallel microfluidic channels and generates ion enrichment in one channel and deletion in the other channel. When ion depletion occurs, the non-uniform electric field induces an electrical force that pushes negative ions away from the depleted region. Subsequently, electro-osmotic flow (EOF), induced by the potential difference between the two terminals of the microfluidic channel, brings ions to the boundary of the depleted region. Nanofluidic preconcentration is able to collect negative ions and macromolecules in a small area of the microfluidic channel (Kwak et al. 2011; Ko et al. 2012; Fan et al. 2020; Lu et al. 2021).

The challenge when using a nanofluidic preconcentrator to enhance the limit of detection (LOD) of an SPR biosensing chip is that SPR sensing chips have to align with the specific area where protein enrichment occurs. Normally, the alignment issue is the key point of the yield rate of mass-production. In this study, we developed a hot-embossing method that is able to simultaneously print microstructures and nanostructures onto plastic thin films. The microstructures can be used as microfluidic channels after bonding, and the nanostructures can be used to generate SPR signals after depositing a thin metal film. The advantage of the co-printing micro/nanostructure method is that the microfluidic channel and SPR sensing chip can automatically be aligned during printing. Further, we also used the fabricated microfluidic device to generate ICP phenomena to collect proteins in the SPR sensing area to enhance the LOD.

2 Materials and methods

2.1 Micro/nanostructural mold preparation

A micro/nanostructural mold was made by two-time lithography including e-beam lithography and traditional photolithography. For e-beam lithography, schematics of the fabrication process are plotted in Fig. 1a–e. First, a 4-inch (10.2-cm) wafer was cleaned with piranha solution (H_2SO_4: $H_2O_2 = 3$: 1) for 30 min, rinsed with deionized (DI) water, dried with a nitrogen stream, and baked in a 120 °C oven for 10 min. ZEP520A was spin-coated onto a cleaned wafer at

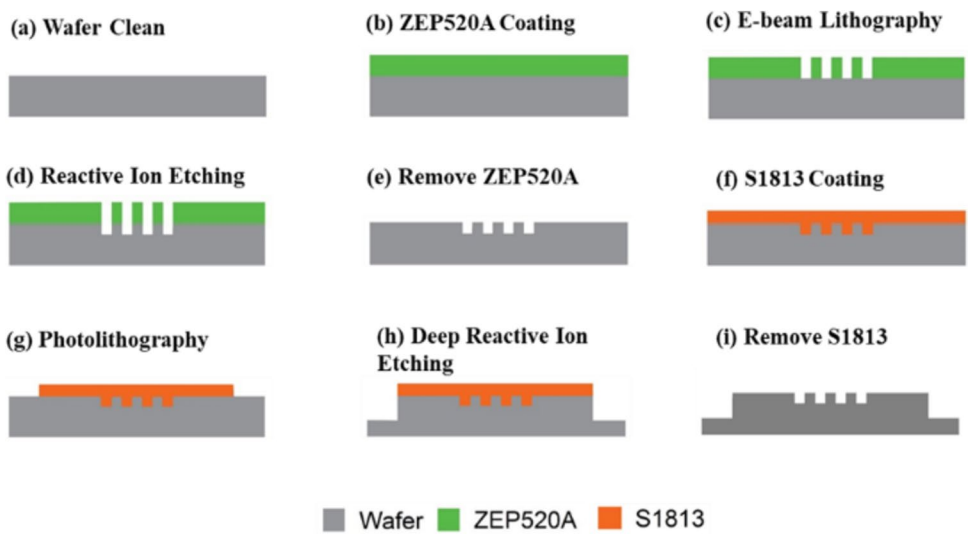

Fig. 1 Procedures of micro/nanostructural mold fabrication. **a** Clean silicon wafer, **b** spin-coating of the ZEP520A photoresist, **c** patterning of the photoresist by e-beam lithography, **d** etching of the silicon substrate by reactive ion etching (RIE), **e** removal of the photoresist, **f** spin-coating of the s1813 photoresist, **g** patterning of the photoresist with a photomask and aligner, **h** etching of the silicon substrate by deep RIE, and **i** removal of the s1813 photoresist, and then cleaning of the substrate to obtain the finished mold

a rotating speed of 6000 rpm for 120 s to obtain a 300-nm-thick photoresist. The ZEP520A-coated wafer was then baked on a 180 °C hotplate for 3 min to evaporate the solvent. The photoresist was patterned with an e-beam writer (ELS7500, Elionix, Tokyo, Japan) at 100 kV and an exposure area dose of 200 μC/cm^2. After lithography, the e-beam-patterned ZEP520A was developed using ZED-N50 developer for 1 min, and then rinsed with ZMD-D for 10 s. The wafer was further baked using a 140 °C hotplate for 3 min. After baking, the wafer was subjected to reactive ion etching (RIE) for 2 min with an etching gas of 50 sccm CHF_3/25 sccm SF_6, to a depth of 100 nm. To remove the photoresist, piranha solution was used for several minutes, with the wafer left in an ultrasonic machine for 30 min. After drying, the wafer was cut to 38 × 28 mm. In this study, we etched a one-dimensional gap array of 50 nm in width, 500 nm in period, and a total area of 150 × 150 μm. After transferring the pattern to a transparent polymer film by hot embossing, the "nanostructure" on polymer film was called a "nanoslit".

A microfluidic mold was further made on the wafer and aligned with a grate structure. The procedures are shown in Fig. 1f–i. The S1813 photoresist was spin-coated onto the substrate at a rotating speed of 2000 rpm for 30 s, and baked on a 120 °C hotplate for 1 min. The photomask of the microfluidic channel was aligned to two nanostructural arrays and exposed to an energy dose of 180 mJ/cm^2 for 17 s. After exposure, the substrate was immersed in developer of 2% tetramethyl ammonium hydroxide (TMAH) for 40 s, and then baked on a 120 °C hotplate for 10 min. The S1813 patterned substrate was then dry-etched by inductively coupled plasma (ICP)-RIE with 1:1 C_4F_8: SF_6 gases for 3 h. A microfluidic mold depth of 10 μm was obtained. After etching, the photoresist was removed with piranha solution and ultrasonic treatment for 30 min, and then rinsed with DI water. After rinsing and drying, the substrate was ready to use.

2.2 Hot-embossing process

The fabricated micro/nanostructure shown in Fig. 2a was used as a mold for hot embossing. The micro/nanostructure hybrid mold on a silicon substrate was designed and fabricated as shown in Fig. 2b. The COP film (ZF16-188, ZeonorFilm, Zeon Corp., Kawasaki City, Japan) with a thickness of 188 μm was cut to 3 × 4 cm, sandwiched between the mold and a flat glass wafer, and placed into the hot-embossing machine. Initially, the top/bottom plates were set to heat up to 180/140 °C, and a pressure of 0.20 MPa was provided for 90 s. After releasing the pressure, the top/bottom plates were cooled to 100/80 °C, and then the COP film was peeled off the mold as shown in Fig. 2c.

2.3 Nafion patterning process

To create an ion-selective channel across two parallel channels, a nanoporous thin membrane, called Nafion, was patterned using a microfluidic deposition method. A flow chart of the process is shown in Fig. 3. First, a microgroove was made with polydimethylsiloxane (PDMS) using regular soft lithography. The PDMS groove covered the area where we desired to pattern Nafion onto the COP substrate, and was

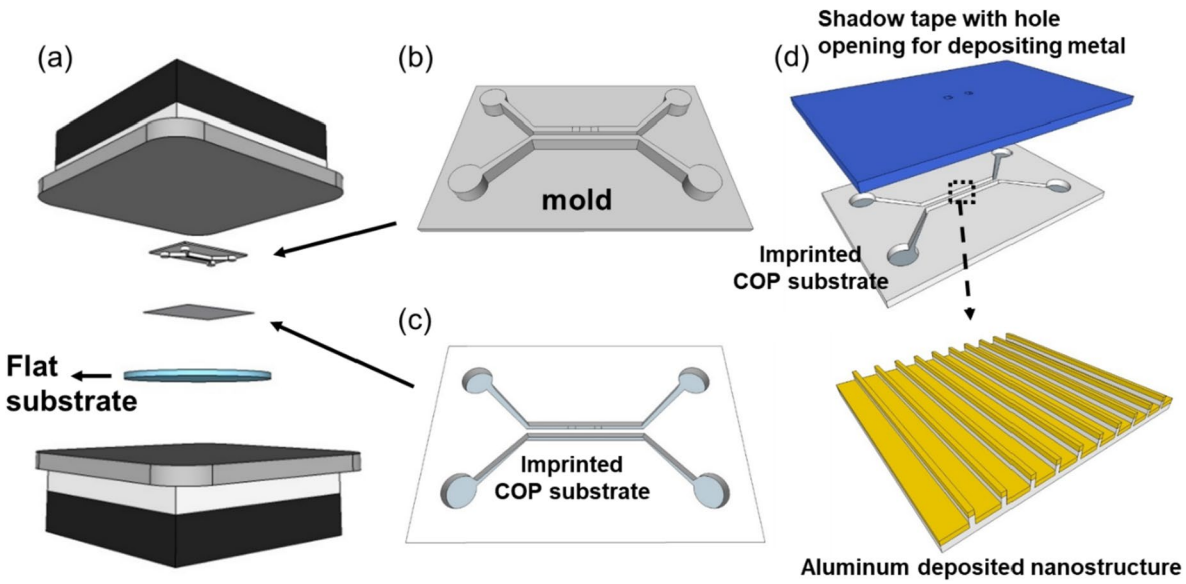

Fig. 2 Schematics of the hot-embossing technique for co-printing the nanostructure and microstructure. **a** Two flat stages clamped, **b** the mold and **c** plastic film and also increased the temperature. **d** After printing, the nanostructures on the plastic substrate were deposited with thin aluminum by covering with shadow tape and sputter-coating

temporarily bonded to the substrate. The Nafion membrane was patterned near the SPR sensing area, thus bridging the two parallel channels on the COP substrate.

To generate the ion concentration polarization (ICP) phenomenon, the Nafion thin film, a nanoporous membrane, was patterned between two nanoslit structures through a microflow pattering technique as shown in Fig. 1c. First, the designed PDMS-based microfluidic channel was aligned and temporarily bonded to the nanoslit substrate. Nafion which had been dissolved in a mixture of low-aliphatic alcohols, and water was allowed to flow into the microfluidic channel. After 30 s, the microfluidic channel was removed. The patterned thin Nafion membrane was successfully deposited onto the nanoslit substrate after solution volatilization.

2.4 Experimental setup

The experimental setup included a power supply to trigger ICP in the microfluidic channel, a spectrometer to measure resonant wavelength spectra of the nanoslit SPR sensor in the microfluidic channel, and a computer to record and analyze variations in the resonant wavelength spectra. To sense biomolecules by nanoslit SPR, resonant wavelength spectra of the nanoslit SPR were measured with a spectrometer. A white light was focused by a 10 × objective lens onto the nanoslit SPR sensing region, and the transmitted light was collected by another 10 × objective lens from the opposite side of the SPR sensing chip. The light was polarized in the transverse-magnetic (TM) direction, and spectra were recorded in real time with a spectrometer. Variations in the peaks of the resonant spectra were analyzed by a computer. To observe preconcentration plug formatting in the microfluidic channel, an inverted fluorescence microscope with a 10 × objective lens was used, and images were recorded with a camera (Fig. 4).

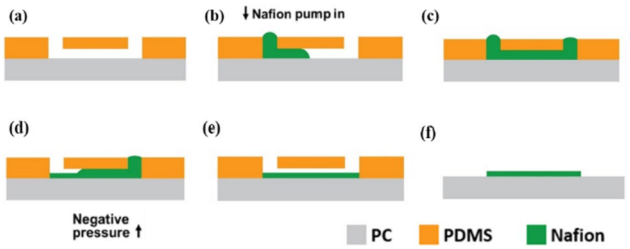

Fig. 3 Processes of Nafion thin-film deposition by a microfluidic patterning method. **a** A microfluidic channel was designed and placed on the substrate without permanent bonding. **b** Nafion dissolved in alcohol was allowed to flow by capillary action into the channel. **c** After the Nafion solution had filled the microfluidic channel, it was incubated for 30 s. **d** After incubation, the Nafion solution was aspirated out of the microfluidic channel. **e** When aspirating out the Nafion solution, a thin film of Nafion was left as a residual in the channel. **f** After drying and removing the microfluidic channel, the thin Nafion film was patterned on the substrate

2.5 Integrated device

To fabricate this device, the microfluidic channel and nanoslit structure were first co-printed by hot embossing, and then nanoslit structures were deposited as an aluminum (Al) film with a thickness of 50 nm by a thermal evaporator and as a thin layer of aluminum oxide (AlO_2) by atom layer deposition. A Nafion thin film was patterned between the two SPR sensing regions after Al deposition. The Nafion film also crossed the two parallel channels. Four holes were drilled into a piece of cured, flat PDMS, which were used to connect to the channel inlets and outlets. PDMS was used to seal the microstructure to form microfluidic channels. To bond the PDMS and COP substrate together, the COP substrate and 0.3 ml 99% v/v of a 3-aminopropyl triethoxysilane (APTES) ethanol solution were left in a vacuum chamber overnight for vapor deposition of the APTES onto the COP and AlO_2 surface. After APTES deposition, PDMS and the COP substrate were treated with oxygen plasma at 18 W for 30 s, and PDMS and the COP substrate were bonded together.

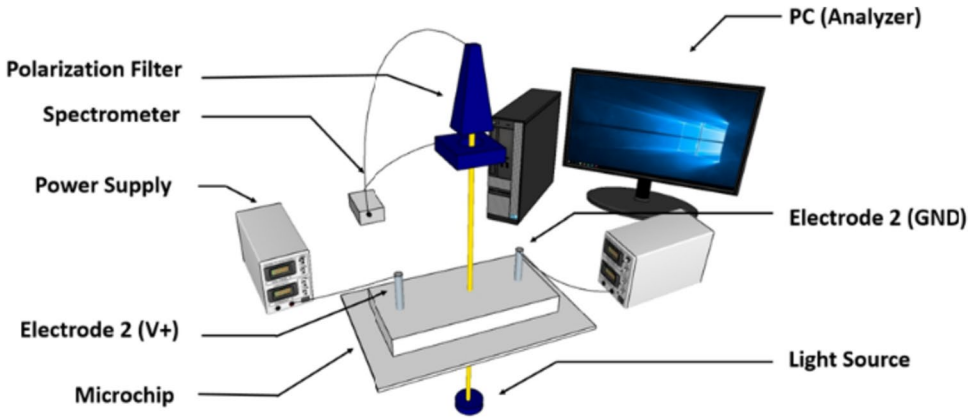

Fig. 4 Setup for preconcentration and surface plasmon resonance (SPR) detection

3 Sensing theory

When a light penetrates a periodic metallic nanostructure in one dimension, the resonant wavelength (λ) in the TM direction is described by

$$\lambda = a \cdot d_p; \tag{1}$$

where a is the environmental refractive index near the SPR sensing region, and d_p is the period of the metallic nanostructure. For example, when an SPR sensing chip is in air, the refractive index of the air is 1, so that the value of the resonant peak is equal to the period of the nanostructure. When an SPR chip is immersed in water, the environmental refractive index is 1.33. To detect biomolecules with an SPR sensing chip, bovine serum albumin (BSA) was first modified to the SPR surface by van der Waals forces. The BSA adherent on the metallic SPR surface caused the environmental refractive index to increase, the resonant peak to be red-shifted, and the peak value to increase. The BSA adherent on the SPR surface was affinity-conjugated with anti-BSA, and the peak value increased again. To quantify biomolecules, different concentrations of anti-BSA samples were prepared, and the red-shift of the SPR chip was quantified (Fig. 5).

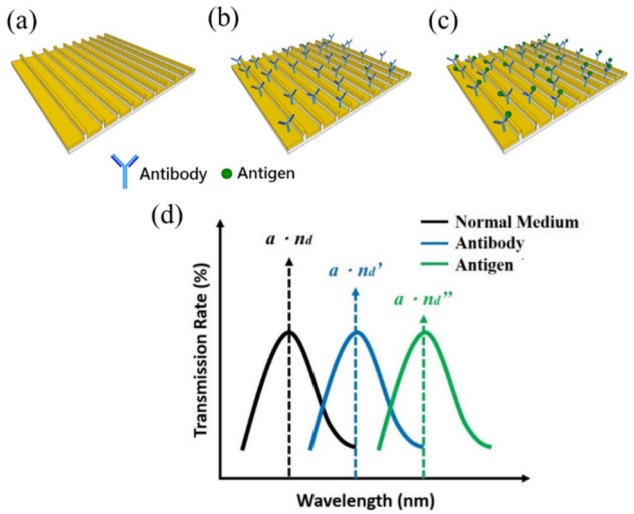

Fig. 5 Mechanism of macromolecule detection based on a surface plasmon resonance (SPR) sensing chip. **a** A bare SPR chip, **b** an antibody-modified SPR chip, **c** an antibody-modified SPR chip interacting with an antigen, and **d** resonant peaks showing a red-shift when conjugating increasing numbers of macromolecules

4 Results and discussion

4.1 Calibration of the Al-nanoslit SPR sensing chip in the microfluidic channel

To calibrate the Al-based nanoslit SPR sensing chip in the microfluidic channel, different concentrations of glycerol solutions in a range of 0–20% v/v were prepared. The glycerol solutions were allowed to sequentially flow into the microfluidic channel, and resonant waveforms of the SPR sensing area were recorded. After curve fitting and normalization, overlapping waveforms were plotted in Fig. 6a. Different concentrations of glycerol solutions corresponding to refractive indexes can be found at a website (www.dow.com/glycerine/resources). When higher concentration glycerol solutions flowed into the microfluidic channel, the SPR spectrum in the TM wave direction exhibited a greater red-shift because of the higher refractive index. To evaluate the sensitivity of the developed SPR sensor, peak values of the resonant waves shown in Fig. 6a were plotted on the

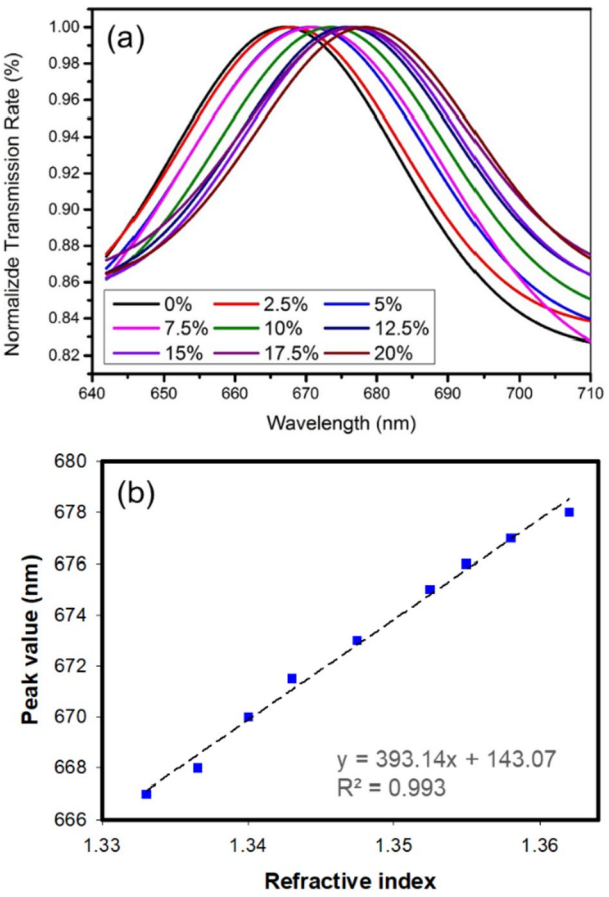

Fig. 6 Sensitivity test. **a** Resonant peaks of surface plasmon resonance (SPR) chips immersed in different-concentration glycerol solutions. **b** Peak values associated with the refractive index

x-axis, and the refractive indexes corresponding to concentrations of glycerol solutions of resonant waves were plotted on the y-axis, as shown in Fig. 6b. Peak values showed linear relations to the refractive index. Based on these results, a wavelength sensitivity of 393 nm/refractive index unit (RIU) was found.

After being modified with APTES, aluminum oxide on the nanoslit was able to conjugate with amino groups on proteins through carboxyl groups at the end of APTES. In this study, BSA diluted in phosphate-buffered saline (PBS) at a final concentration of 1 mg/ml was first allowed to flow into the microfluid channel and was retained for 2 h. After incubation, we continuously flushed the microfluid channel with PBS for 5 min to wash out non-specific bound BSA. Different concentrations of anti-BSA solutions in PBS from 20 ng/ml to 200 µg/ml were prepared to demonstrate the sensing technique. Prepared samples were allowed to sequentially flow into the microfluid channel from low to high concentrations. Each sample flowed into the microfluidic channel for 10 min at a flow rate of 1 µL/min, and the resonant spectrum of the SPR chip was recorded. After smoothing and normalization, the spectra were stacked as in Fig. 7a. Results indicated that the SPR sensing area in the microfluidic channel conjugated more anti-BSA when higher concentrations of anti-BSA samples flowed into the device. With more anti-BSA attached to the BSA on the SPR sensing area, the environmental refractive index more strongly changed, resulting in a greater red-shift of the resonant peak wavelength. We repeated the experiment three times, recorded the resonant peak wavelength for each condition, and plotted the red-shift in Fig. 7b. Experimental data points of the red-shift versus anti-BSA concentration on a logarithmic scale plot were linearly regressed and showed an R^2 value of 0.97.

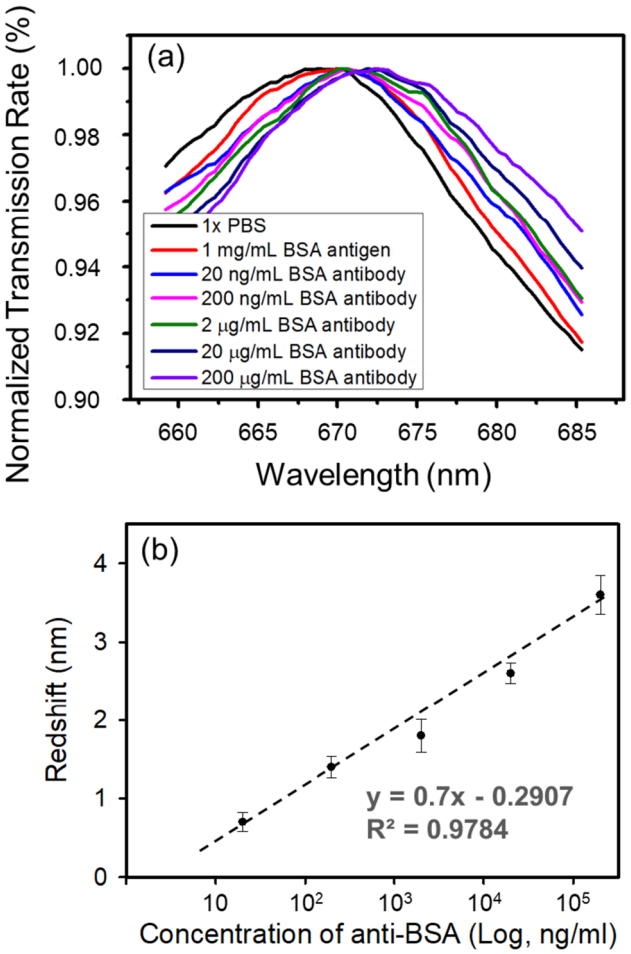

Fig. 7 Macromolecule detection. **a** Stacked spectra of resonant wavelengths for detecting different concentrations of the bovine serum albumin (BSA) antibody. **b** Red-shift of peak values versus concentrations of antibody on a logarithmic scale

4.2 Preconcentration in the microfluidic channel

Our strategy to improve the detection limit and sensitivity of the SPR sensing chip was to enrich targeted samples in the sensing region. The developed microfluidic device shown in Fig. 8 was used. To electrically manipulate anti-BSA in the microfluidic channel, an initial voltage of 5 V was applied to the two terminals of the main channel, and the two terminals of the buffer channel were grounded. Two power supplies and two sides of the terminals of the main and buffer channels formed two circuits, named the left and right circuits. As to electrical conditions, ion depletion occurred in the intersecting region of the main channel and ion-selective channel. The ion-depletion phenomenon resulted in a non-uniform electric field and an electric force that pushed molecules or proteins with a negative charge away from the depletion region.

Subsequently, we increased the voltage of the left circuit to 10 V, and the voltage difference between the left and right circuits generated EOF in the main channel, which flowed from the left to the right side. The EOF brought ions, molecules, and proteins to the boundary of the ion-depletion region, and those with a negative charge were excluded from the depletion region in the main channel. Therefore, proteins with a negative charge were trapped near the ion-depletion region.

In this experiment, fluorescein 5-isothiocyanate (FITC)-conjugated goat anti-mouse immunoglobulin G (IgG; 31569, Thermo Fisher Scientific) was used to visualize the protein-trapping processes. The trapping processes are shown in Fig. 9. First, a 5.8 nM fluorescent antibody was prepared and allowed to flow into the main channel of the device as shown in Fig. 9a. When we applied 5 V to the left and right circuits, a deletion region occurred and grew until it occupied all of the intersecting region of Nafion and the microfluidic channel, and pushed proteins away as shown in Fig. 9b and c. In the next step, we increased the voltage of the left circuit to

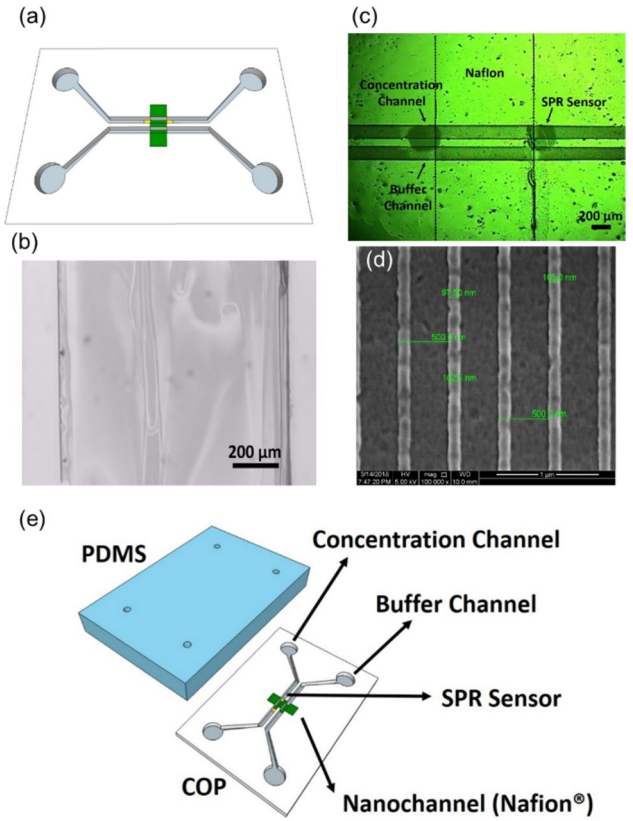

Fig. 8 Preconcentration of an integrated surface plasmon resonance (SPR) sensing chip. **a** Nafion patterning near the SPR chip. **b** Image of patterned Nafion. **c** Image of the SPR chip integrated with the microfluidic channel and preconcentrator. **d** SEM image of the nanostructure of the SPR chip. **e** Configuration of the sensing chip with preconcentration

10 V, and a protein-concentrated plug was observed near the left side of the Nafion as shown in Fig. 9d where the SPR sensor was located.

The developed preconcentrating device was used to enhance SPR signals. We loaded anti-BSA samples from 20 ng/ml to 20 µg/ml into the device. After the preconcentration process and incubation for 10 min, we measured SPR signals and calculated the red-shift for each case. Average results were plotted and compared to those shown in Fig. 7b. As shown in Fig. 10, we found that after preconcentration, the red-shift of the SPR resonant peaks had increased 1 ~ 1.9 nm on average compared to those without preconcentration.

From data shown in Fig. 10, anti-BSA with concentrations of 20, 200, 2000, 20,000 and 200,000 ng/ml without preconcentration caused resonant peaks of SPR signals to red-shift 0.7, 1.4, 1.8, 2.6, and 3.6 nm, respectively. After preconcentrating, the 20, 200, and 2000 ng/ml anti-BSA samples on SPR chips caused resonant peaks to red-shift 1.7, 2.4, and 3.3 nm, respectively, which were close to the shifting results from the 2000, 20,000 and 200,000 ng/ml samples without preconcentrating. Therefore, we estimated that our preconcentrating device was able to enrich anti-BSA by 100-fold.

Results indicated that the preconcentrator helped enhance SPR signals, because proteins in the microfluidic channel collected at the SPR sensing region accelerated BSA and anti-BSA interactions. With traditional biosensors, targets are transported to the sensing region through diffusion; therefore, it takes a long time for the reaction to occur. In contrast, the electrical preconcentrating technique forces them to rapidly encounter each other, and they interact much more quickly.

Development of metallic nanostructures for generating LSPR signals can be separated into two ways: (1) chemical synthesis of nanoparticles (NPs) on a substrate, and (2) nanofabrication on a substrate. For chemical synthesis of NPs, previous work studied LSPR signals of synthesized NPs with different composite materials (Sui et al. 2019; Jian et al. 2020; Yu et al. 2020) and shape effects (Kuo et al. 2017; Yougbaré et al. 2021). Studies using nanofabrication mainly focused on effects from structural shapes (Xu and Geng 2021), and interactions between two structures (Hsiao et al. 2020; Chang et al. 2021). These efforts mentioned above optimized the sensitivity and detection limit of their nanoplasmonic chips. To integrate nanoplasmonic chips with microfluidic channels for the continuous monitoring of LSPR signals, the microfluidic channels need to be aligned and bonded to the developed substrates, and well-trained technicians are required (Geng et al. 2014; Soler et al. 2017).

In our study, the strategy we used to improve the detection limit was to preconcentrate the sample in the microfluidic channel. Further, we together printed the nanostructure for LSPR sensing and the microstructure for building the microfluidic channel. By co-printing them together, we did not need to align the LSPR sensing chip and the microfluidic channel. A comparison is shown in Table 1.

5 Conclusions

In this study, we developed a nanostructure/microstructure co-printing technique that can respectively be used to produce SPR sensing chips and microfluidic channels. With co-printing, the alignment procedure of the microfluidic channel to the SPR chip can be omitted during manufacture, which can dramatically increase the fabrication yield rate. The SPR sensing chip embedded in the microfluidic device and integrated with the nanofluidic preconcentrator demonstrated enhanced macromolecule detection. The peak of the resonance spectrum of the SPR chip was measured. Peak values versus different concentrations of glycerol solutions were plotted to determine a refractive index sensitivity of 393 nm/RIU. After modifying BSA on the surface of the

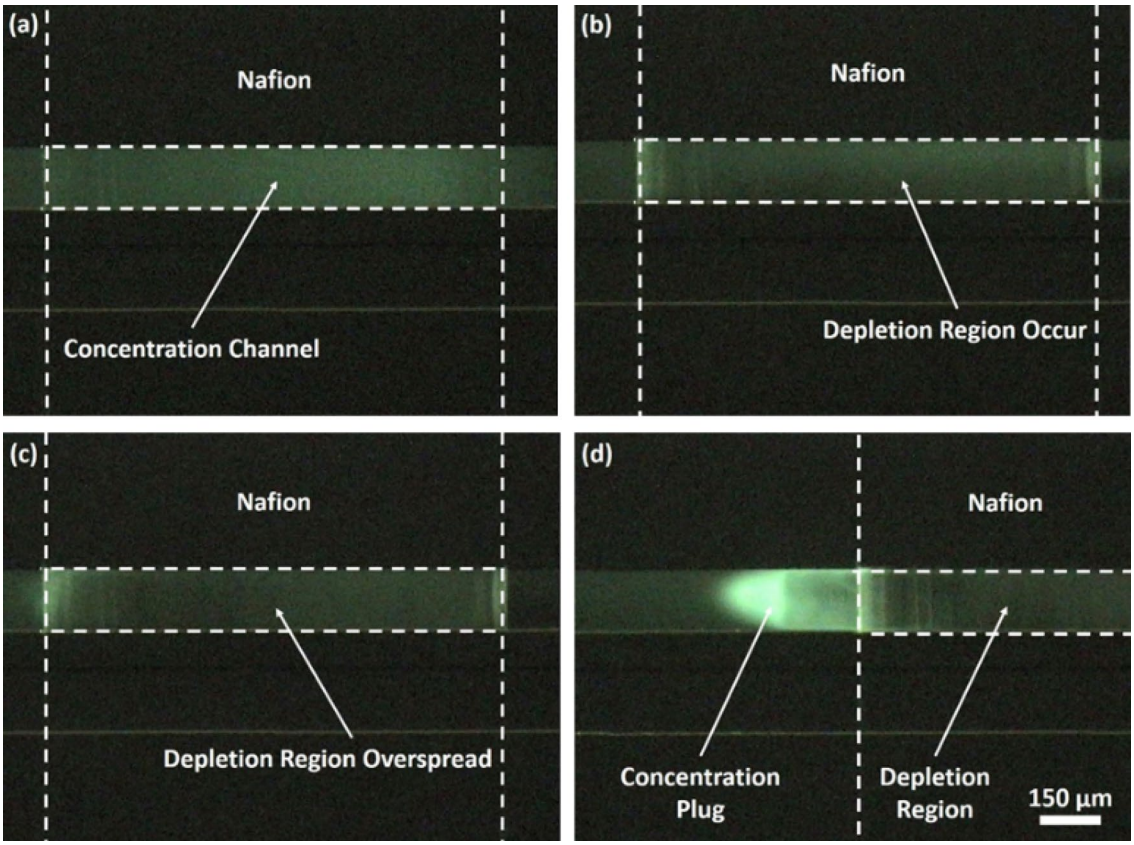

Fig. 9 Nanofluidic concentration processes. **a** A fluorescent dye-labeled protein solution filled the sample channel. **b** When voltage was applied, ion-deletion occurred. **c** The voltage was increased until a depletion region overlapped the entire microfluidic channel where it intersected the Nafion. **d** Applying a voltage difference between the two ends of the sample channel caused a concentration plug to occur near the Nafion

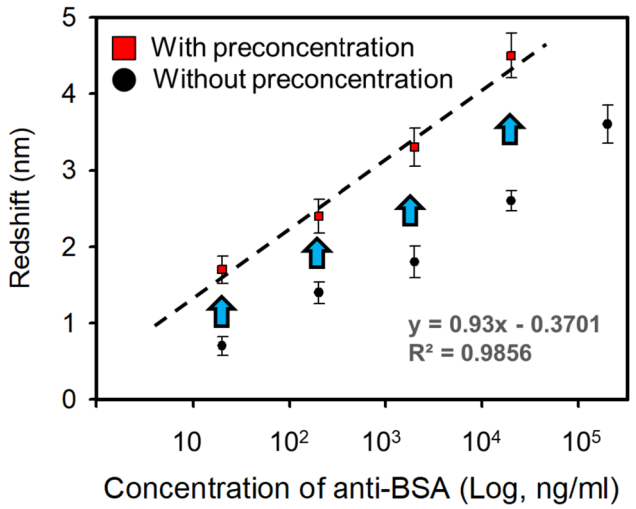

Fig. 10 Comparison of anti-bovine serum albumin (BSA) detection with and that without preconcentration

SPR sensing area, different concentrations of anti-BSA samples were allowed to flow into the device and were incubated for a period to allow BSA and anti-BSA to interact. After the BSA and anti-BSA interacted, the resonant wavelengths of the SPR chip red-shifted. Distances that peak values of the resonant wavelengths shifted after BSA interacted with different concentrations of anti-BSA were obtained to build a standard curve. We also preconcentrated anti-BSA in the SPR sensing chip region, incubated it for a period, and then measured peak values of resonant wavelengths. Moreover, a comparison of anti-BSA detection with and that without preconcentration was investigated, and a preconcentration factor of around 100-fold was found.

Table 1 Comparison of the current method to other techniques

Type	Fabrication method	Sensing improvement strategy	Microfluidic integration	Reference
Nanoparticles	Chemical synthesis	Composite materials, nanoparticle shape	Alignment needed	(Geng et al. 2014; Sui et al. 2019)
Nanostructures	Nanofabrication	Effect of shape and interaction between two structures	Alignment needed	(Soler et al. 2017; Xu and Geng 2021)
Nanostructures	Hot embossing	Integration with a preconcentrator	Fabricated together	Current study

Acknowledgements This work was supported by the National Science and Technology Council of Taiwan (grant nos. NSTC 112-2636-E-038-003, 111-2221-E-002-128, and 111-2811-E-002-030), and by Taipei Medical University Hospital (grant no. 112TMU-TMUH-07). We would also like to thank the NEMS Research Center, National Taiwan University for facility support.

Author contributions Y-JL, H-JS, Y-JF fund the project. Y-JL, and H-YH analyze the data, and draft the manuscript. W-FY collected the data. K-CW, HT provided the idea and proof the analyzed data. P-KW provided the idea and technique of fabrication. H-JS and Y-J Fan provide the fabrication skill, and finalized the manuscript. All authors reviewed the manuscript.

Funding Taipei Medical University Hospital, 112TMU-TMUH-07, National Science and Techology Council of Taiwan, NSTC 111-2811-E-002 -030, NSTC 111-2221-E-002 -128, NSTC 112-2636-E-038 -003.

Data availability The data that support the findings of this study are available from the corresponding author upon reasonable request.

Declarations

Conflict of interest The authors declare no competing interests.

References

Chang Y-C, Dvoynenko MM, Ke H et al (2021) Double resonance SERS substrates: Ag nanoparticles on grating. J Phys Chem C 125:27267–27274. https://doi.org/10.1021/acs.jpcc.1c07454

Chuang C-S, Wu C-Y, Juan P-H et al (2020) LMP1 gene detection using a capped gold nanowire array surface plasmon resonance sensor in a microfluidic chip. Analyst 145:52–60. https://doi.org/10.1039/C9AN01419E

Chung P-S, Fan Y-J, Sheen H-J, Tian W-C (2015) Real-time dual-loop electric current measurement for label-free nanofluidic preconcentration chip. Lab Chip. https://doi.org/10.1039/c4lc01143k

Das S, Devireddy R, Gartia MR (2023) Surface plasmon resonance (SPR) sensor for cancer biomarker detection. Biosensors (basel) 13:396. https://doi.org/10.3390/bios13030396

Deng C-Z, Fan Y-J, Chung P-S, Sheen H-J (2018) A novel thermal bubble valve integrated nanofluidic preconcentrator for highly sensitive biomarker detection. ACS Sens 3:1409–1415. https://doi.org/10.1021/acssensors.8b00323

Dutta P, Su T-Y, Fu A-Y et al (2022) Combining portable solar-powered centrifuge to nanoplasmonic sensing chip with smartphone reader for rheumatoid arthritis detection. Chem Eng J 434:133864. https://doi.org/10.1016/j.cej.2021.133864

Ebbesen TW, Lezec HJ, Ghaemi HF et al (1998) Extraordinary optical transmission through sub-wavelength hole arrays. Nature 391:667–669. https://doi.org/10.1038/35570

Fan Y-J, Deng C-Z, Chung P-S et al (2018) A high sensitivity bead-based immunoassay with nanofluidic preconcentration for biomarker detection. Sens Actuators B Chem 272:502–509. https://doi.org/10.1016/j.snb.2018.05.141

Fan Y-J, Huang M-Z, Hsiao Y-C et al (2020) Enhancing the sensitivity of portable biosensors based on self-powered ion concentration polarization and electrical kinetic trapping. Nano Energy 69:104407. https://doi.org/10.1016/j.nanoen.2019.104407

Geng Z, Kan Q, Yuan J, Chen H (2014) A route to low-cost nanoplasmonic biosensor integrated with optofluidic-portable platform. Sens Actuators B Chem 195:682–691. https://doi.org/10.1016/j.snb.2014.01.110

Homola J, Piliarik M (2006) Surface plasmon resonance (SPR) sensors. Springer Ser Chem Sens Biosens 4:45–67. https://doi.org/10.1007/5346_014

Homola J, Yee SS, Gauglitz G (1999) Surface plasmon resonance sensors: review. Sens Actuators B Chem 54:3–15. https://doi.org/10.1016/S0925-4005(98)00321-9

Hsiao H-H, Ke H, Dvoynenko MM, Wang J-K (2020) Multipolar resonances of ag nanoparticle arrays in anodic aluminum oxide nanochannels for enhanced hot spot intensity and signal-to-background ratio in surface-enhanced Raman scattering. ACS Appl Nano Mater 3:4477–4485. https://doi.org/10.1021/acsanm.0c00569

Hsieh H-Y, Chang R, Huang Y-Y et al (2022a) Continuous polymerase chain reaction microfluidics integrated with a gold-capped nanoslit sensing chip for Epstein-Barr virus detection. Biosens Bioelectron 195:113672. https://doi.org/10.1016/j.bios.2021.113672

Hsieh H-Y, Luo J-X, Shen Y-H et al (2022b) A nanofluidic preconcentrator integrated with an aluminum-based nanoplasmonic sensor for Epstein-Barr virus detection. Sens Actuators B Chem 355:131327. https://doi.org/10.1016/j.snb.2021.131327

Jian C, Zhang J, Ma X (2020) Cu–Ag alloy for engineering properties and applications based on the LSPR of metal nanoparticles. RSC Adv 10:13277–13285. https://doi.org/10.1039/D0RA01474E

Ko SH, Song YA, Kim SJ et al (2012) Nanofluidic preconcentration device in a straight microchannel using ion concentration polarization. Lab Chip. https://doi.org/10.1039/c2lc21238b

Kuo T-R, Chen Y-C, Wang C-I et al (2017) Highly oriented Langmuir-Blodgett film of silver cuboctahedra as an effective matrix-free sample plate for surface-assisted laser desorption/ionization mass spectrometry. Nanoscale 9:11119–11125. https://doi.org/10.1039/C7NR04098A

Kwak R, Kim SJ, Han J (2011) Continuous-flow biomolecule and cell concentrator by ion concentration polarization. Anal Chem. https://doi.org/10.1021/ac2012619

Lee K-L, Chen P-W, Wu S-H et al (2012) Enhancing surface plasmon detection using template-stripped gold nanoslit arrays on plastic films. ACS Nano 6:2931–2939. https://doi.org/10.1021/nn3001142

Lee K-L, Huang J-B, Chang J-W et al (2015) Ultrasensitive biosensors using enhanced fano resonances in capped gold nanoslit arrays. Sci Rep 5:8547. https://doi.org/10.1038/srep08547

Lee K-L, You M-L, Tsai C-H et al (2016) Nanoplasmonic biochips for rapid label-free detection of imidacloprid pesticides with a smartphone. Biosens Bioelectron. https://doi.org/10.1016/j.bios.2015.08.010

Lee K-L, You M-L, Wei P-K (2019) Aluminum nanostructures for surface-plasmon-resonance-based sensing applications. ACS Appl Nano Mater 2:1930–1939. https://doi.org/10.1021/acsanm.8b02325

Lezec HJ, Degiron A, Devaux E et al (2002) Beaming light from a subwavelength aperture. Science 297:820–822. https://doi.org/10.1126/science.1071895

Lu Y-J, Hsieh H-Y, Kuo W-C et al (2021) Nanoplasmonic structure of a polycarbonate substrate integrated with parallel microchannels for label-free multiplex detection. Polymers (basel) 13:3294. https://doi.org/10.3390/polym13193294

Mahmoudpour M, Ezzati Nazhad Dolatabadi J, Torbati M et al (2019) Nanomaterials and new biorecognition molecules based surface plasmon resonance biosensors for mycotoxin detection. Biosens Bioelectron 143:111603. https://doi.org/10.1016/j.bios.2019.111603

Masson J-F (2017) Surface plasmon resonance clinical biosensors for medical diagnostics. ACS Sens. https://doi.org/10.1021/acssensors.6b00763

Mostufa S, Akib TBA, Rana MdM, Islam MdR (2022) Highly sensitive TiO2/Au/graphene layer-based surface plasmon resonance biosensor for cancer detection. Biosensors (basel) 12:603. https://doi.org/10.3390/bios12080603

Mousavi M, Chen H-Y, Hou H-S et al (2015) Label-free detection of rare cell in human blood using gold nano slit surface plasmon resonance. Biosensors (basel) 5:98–117. https://doi.org/10.3390/bios5010098

Sheen H-J, Panigrahi B, Kuo T-R et al (2022) Electrochemical biosensor with electrokinetics-assisted molecular trapping for enhancing C-reactive protein detection. Biosens Bioelectron 210:114338. https://doi.org/10.1016/j.bios.2022.114338

Sherry LJ, Chang S-H, Schatz GC et al (2005) Localized surface plasmon resonance spectroscopy of single silver nanocubes. Nano Lett 5:2034–2038. https://doi.org/10.1021/nl0515753

Singh P (2016) SPR biosensors: historical perspectives and current challenges. Sens Actuators B Chem 229:110–130

Soler M, Belushkin A, Cavallini A et al (2017) Multiplexed nanoplasmonic biosensor for one-step simultaneous detection of *Chlamydia trachomatis* and *Neisseria gonorrhoeae* in urine. Biosens Bioelectron 94:560–567. https://doi.org/10.1016/j.bios.2017.03.047

Stewart ME, Anderton CR, Thompson LB et al (2008) Nanostructured plasmonic sensors. Chem Rev 108:494–521. https://doi.org/10.1021/cr068126n

Sui M, Kunwar S, Pandey P, Lee J (2019) Strongly confined localized surface plasmon resonance (LSPR) bands of Pt, AgPt, AgAuPt Nanoparticles. Sci Rep 9:16582. https://doi.org/10.1038/s41598-019-53292-1

Tan S-H, Yougbaré S, Tao H-Y et al (2021) Plasmonic gold nanoisland film for bacterial theranostics. Nanomaterials 11:3139. https://doi.org/10.3390/nano11113139

Wang YC, Stevens AL, Han J (2005) Million-fold preconcentration of proteins and peptides by nanofluidic filter. Anal Chem. https://doi.org/10.1021/ac050321z

Wang S-H, Lo S-C, Tung Y-J et al (2020) Multichannel nanoplasmonic platform for imidacloprid and fipronil residues rapid screen detection. Biosens Bioelectron 170:112677. https://doi.org/10.1016/j.bios.2020.112677

Xu T, Geng Z (2021) Strategies to improve performances of LSPR biosensing: Structure, materials, and interface modification. Biosens Bioelectron 174:112850. https://doi.org/10.1016/j.bios.2020.112850

Yougbaré S, Mutalik C, Krisnawati DI et al (2020) Nanomaterials for the photothermal killing of bacteria. Nanomaterials 10:1123. https://doi.org/10.3390/nano10061123

Yougbaré S, Chou H-L, Yang C-H et al (2021) Facet-dependent gold nanocrystals for effective photothermal killing of bacteria. J Hazard Mater 407:124617. https://doi.org/10.1016/j.jhazmat.2020.124617

Yu X, Liu X, Wang B et al (2020) An LSPR-based "push–pull" synergetic effect for the enhanced photocatalytic performance of a gold nanorod@cuprous oxide-gold nanoparticle ternary composite. Nanoscale 12:1912–1920. https://doi.org/10.1039/C9NR08808C

Zhao J, Zhang X, Yonzon CR et al (2006) Localized surface plasmon resonance biosensors. Nanomedicine 1:219–228

Zhou J, Qi Q, Wang C et al (2019) Surface plasmon resonance (SPR) biosensors for food allergen detection in food matrices. Biosens Bioelectron 142:111449